



TECHNICAL ARTICLE

Effect of Die Design and Sheet Placement on Self-Piercing Rivet of Automotive Steels and Comparison with Resistance Spot and Friction Stir Spot Welding

Brajesh Asati , R. Ganesh Narayanan, Nikhil Shajan, and Kanwer Singh Arora

Submitted: 14 September 2022 / Revised: 29 November 2022 / Accepted: 10 December 2022 / Published online: 27 December 2022

The present work addresses the impact of die design (flat die or pip die) and sheet placement on the self-piercing riveting (SPR) of automotive grade CR210 and CR340 galvanized steel sheets. Actual rivet head height, interlock distance, bottom sheet thickness, maximum riveting force, lap-shear fracture load, and fracture modes are monitored. Later, the lap-shear tensile performance of SPR joints is compared with joints made using resistance spot welding (RSW) and friction stir spot welding (FSSW). Both die design and sheet placement impact the SPR outputs significantly. Flat die results in improved rivet penetration irrespective of sheet placement. Maximum riveting force in the case of pip die is higher irrespective of sheet placement. Pip die results in better interlocking than the flat die, irrespective of sheet placement. The effect of die design on lap-shear fracture load and fracture mode is marginal for the sheet combination. However, optimization of sheet placement is critical for SPR. Locating the CR210 (weaker, thinner) sheet at the top would be beneficial if riveting force and interlock distance are referred to. However, if the bottom sheet thickness and tensile-shear fracture load are considered, placing the CR340 (stronger, thicker) sheet on top would be acceptable. Sheet placement has a marginal influence on RSW joint formation and tensile-shear performance. Sheet placement is also critical for FSSW in terms of joint formation. The lap-shear fracture load of RSW joints was higher than that of SPR and FSSW joints. However, SPR joints exhibited significantly higher displacement at fracture than RSW and FSSW.

Keywords die, fracture, galvanized steel, material, self-piercing riveting, spot welding

1. Introduction

Several raw material manufacturers and users developed alliances such as ULSAB to reduce carbon footprint and CO₂ emissions. Regulations imposed by European Union regulators demand reducing CO₂ emissions to about 95 g CO₂/km by 2020. Existing data show that a weight reduction of 100 kg corresponds to an 8–12 g/km reduction in CO₂ emission. At the same time, there is a significant increase in CO₂ emission with an increase in vehicle mass (Ref 1). Several lightweight materials like high-strength steel, aluminum alloys, plastics, and composites were developed, along with new welding methods like laser welding, friction stir welding (FSW), self-pierce riveting (SPR), clinching, and hybrid methods to achieve the expected fuel economy (Ref 2, 3). Developing complex car body components demand suitable joining methods other than the widely accepted resistance spot welding (RSW) (Ref 4),

which has limitations in joining multi-grade materials. Liquid metal embrittlement and several other welding defects, such as expulsion and shrinkage cavity formation, are encountered while spot welding zinc-coated advanced high-strength steel sheets (AHSS) (Ref 5, 6). Beni et al. highlighted the need for higher welding current required for widely used galvanized interstitial-free (IF) steel compared to uncoated steel resulting in higher power consumption (Ref 7). Ashiri et al. optimized the welding parameters, evaluated the mechanical performance of 1-GPa steel, and concluded that weld nugget size and geometry majorly influence the mechanical performance (Ref 8). Further, Kim et al. highlighted that the multi-pulse welding schedule improves spot weldability for ultra-high strength steel sheets (UHSS) through increased nugget size. However, productivity will be affected due to increased welding cycles of such schedules (Ref 9).

Dissimilar sheet quality, including strength, thickness, melting temperature, joint accessibility, cost, coatings, material corrosion resistance, and heat sensitivity of materials, poses further challenges to deciding a suitable joining method (Ref 10). Huang et al. proposed a novel self-riveting friction stir lap welding (SRFSLW) for joining dissimilar steel-aluminum sheets. The strength of SRFSLW joints was 23% higher than conventional FSW. A combination of mechanical and metallurgical bonding contributed to the increased strength of SRFSLW joints (Ref 11, 12). Further, Huang et al. proposed novel friction surfacing-assisted hybrid friction stir welding (FS-HFSW) for joining Ti-Al alloy joints. The higher tensile load of 12.2 kN, equivalent to 85.3% of Al base material, was obtained without tool deformation. However, avoiding the

Brajesh Asati, Nikhil Shajan, and Kanwer Singh Arora, Materials Welding and Joining Research Group, Research and Development, Tata Steel Ltd, Jamshedpur, Jharkhand 831001, India; and **R. Ganesh Narayanan**, Department of Mechanical Engineering, IIT Guwahati, Guwahati 781039, India. Contact e-mails: brajesh.asati@tatasteel.com and 0410brajesh@gmail.com.

intermetallic formed at the interface is generally challenging, negatively affecting mechanical performance (Ref 13).

Mechanical joining processes such as SPR, clinching, and hemming involve plastic deformation of structures without metallurgical bonding before the joint is fabricated. Mechanical joining processes can overcome issues associated with RSW and friction-based joining processes. Advantages include high productivity at low cost, applicable to the multi-material design as there is no melting, and fabrication of joints with sufficient strengths due to strain hardening. However, the joint materials should have good ductility to make defect-free joints (Ref 14). Among these, SPR is a high-speed fastening technique for spot-joining sheet materials. In this process, a tubular rivet penetrates the sheet pairs toward the die opening below the sheets. The upper sheet is pierced (fractured) first, and the lower sheet is deformed to fill the die cavity along with the upper sheet. During the process, the rivet shank is flared outwards to form the interlock required for the joint formation (Ref 15). The lower sheet is prevented from piercing to minimize the corrosion effect. Though advantages such as short joining time, simple equipment, and high tool life enhance the potential application of SPR, disadvantages such as the requirement of double-side access, higher riveting force, and bulging of sheets in the spot restrict its application. A cylindrical rivet is also used in place of a tubular rivet (Ref 15). Several authors have attempted to understand the process mechanism and optimization of SPR parameters for various alloy combinations. Asati et al. studied the effect of actual head height (AHH) (i.e., rivet penetration post-riveting) on steel-steel SPR joints and reported an increase of 28% in lap-shear fracture load when AHH was -0.3 mm instead of 0.0 mm (Ref 16). Deng et al. evaluated the effect of die design, flat bottom die, and pip die with varying center projection on the SPR joint formation and lap-shear performance for aluminum alloy and mild steel combination (Ref 17). Han and Chrysanthou examined the effect of E-coat and Zn coating on the quality and behavior of SPR joints between NG5754, AA5182, and high-strength low alloy (HSLA) steel. Under static loading, both coatings significantly affect joint strength and failure modes (Ref 18).

Karathanasopoulos et al. analyzed the role of rivet (U1500, U1800) grades and sheet material grades on the SPR of AA7075-BA0270 and AA2019/AA7075-F by experiments and numerical modeling. They related successful joint formation to rivet hardness, shank thickness, and die depth (Ref 19). Mori et al. suggested that SPR of Mild steel, a few dual-phase sheets of steel, and AA5xxx sheets can be improved by locating a softer sheet on top due to smooth piercing (Ref 20). SPR joint made on Zn-coated TWIP, and AA5754 or AA6111 was compared with RSW, Kerb Konus Riveting, and EJOWELD joints (Ref 21). It is the sheet strength that decides the joint strength of SPR joints. Du et al. provided design guidelines to realize good steel-aluminum SPR joints in terms of sheet flow stress ratio, thickness ratio, and placement of sheets (Ref 22). A similar attempt has been made by Du et al. (Ref 23) to study the mechanical behavior of aluminum-steel SPR joints under quasi-static and dynamic loading conditions using experiments and 2-D finite element simulations.

Regarding the fatigue performance of steel-aluminum SPR joints, Chung, and Kim, through experiments and numerical simulations, proposed to use the more robust sheet grade as the bottom sheet (Ref 24), which agrees with Mori et al. work (Ref 20). Asati et al. compared SPR and RSW dissimilar steel joints (CR340-CR210 and Dual-phase 590-IF) and reported superior

fatigue performance of SPR joints vis-à-vis RSW joints. The inherent notch and unfavorable microstructure at heat-affected zone led to inferior dynamic performance (Ref 25, 26). Ma et al. attempted to understand the role of die-to-rivet ratio in SPR joint formation of AA6061-T6 and CR4 steel with four/five different thicknesses, however, without changing the placement of sheets and die design (Ref 27). SPR analyses of boron steel and AA5754 sheets were done by Liu et al. through numerical simulations and experiments (Ref 28). Beyond metallic sheets, composites are joined by SPR (Ref 29). Gupta et al. compared the lap-shear joints' performance of FSSW and SPR dissimilar galvanized steels. It was observed that the lap-shear fracture load of SPR joints was higher by about 50% compared to FSSW joints (Ref 30). Further, Bang et al. evaluated the mechanical performance of FSSW joints of AA A356-T6 and SAPH440 steel. The static lap-shear fracture load of SPR joints (7.9 kN) was significantly higher than FSSW joints (3.9 kN) (Ref 31).

Despite significant contributions on SPR of steel to aluminum and other pairs of materials, SPR of coated steel sheets (like galvanized steel) is scarce. Lou et al. provided resistance heat to SPR joint made of AA6061-T6 and hot-dipped galvanized DP590 for enhancing the quality (Ref 32). Recently, Xie et al. proposed theoretical models for calculating the shear capacity of the SPR joints made of galvanized steel sheets after testing 51 SPR joints constituting various failure modes. From the models, it is observed that joint fracture load depends on yield strength and thickness of sheets, rivet length, rivet head diameter, and rivet shank diameter (Ref 33). More details on applications and the latest advances in SPR of sheets are available in Li et al. (Ref 34).

Considering the status of the SPR of galvanized sheets, the present work aims to investigate the effect of die design and sheet placement on the SPR of galvanized steel sheets, such as 0.8 mm thick CR210 steel and 1.2 mm thick CR340 steel. Through laboratory-scale experiments, joint formation and lap-shear test performance are characterized by varying desired head heights (DHH). Some SPR outputs are evaluated. In the later part, FSSW and RSW of base sheets are performed, and lap-shear test performance is compared with SPR joints. Here the main aim is to compare joints made from mechanical joining, SPR, a solid-state welding process, FSSW, and a resistance welding process, RSW. Such comparison is also scarce in the existing literature.

2. Experimental Methodology

2.1 Base Materials

The sheet materials used for experiments are 0.8 mm thick CR210 steel and 1.2 mm thick CR340 steel; both are cold-rolled galvanized steel sheets with a Zn coating weight of 100 gsm. The chemical composition of the sheets is provided in Table 1. The base sheets are subjected to uniaxial tensile tests as per ASTM E8 standard at a nominal crosshead speed of 5 mm/min to evaluate the stress-strain behavior and mechanical properties, as listed in Table 2. The plastic strain ratio describes the anisotropy of sheets and has been evaluated as per ASTM standard E517-19 at 0° , 45° , and 90° to the rolling direction. The average value is shown in Table 2. The microstructure of CR340 and CR210 sheets are fully ferritic, as shown in

Table 1 Chemical composition (wt.%) of sheets

Base material	C	Mn	Al	Ti	Nb	Si	S	P	N, ppm
CR340	0.045	0.86	0.048	...	0.035	0.008	0.006	0.019	27
CR210	0.0019	0.55	0.04	0.053	...	0.003	0.009	0.047	18

Table 2 Mechanical properties of sheets

Base material	Yield strength, MPa	Tensile strength, MPa	Elongation, %	Strain hardening exponent	Average plastic strain ratio
CR340	377 ± 3	431 ± 3	35 ± 0.2	0.19 ± 0.01	0.63 ± 0.03
CR210	209 ± 2	334 ± 5	44 ± 0.8	0.21 ± 0.00	1.95 ± 0.16

Fig. 1(a), and (b). Niobium (Nb) micro-alloyed CR340 steel exhibits a fine grain structure compared to CR210. Figure 1(c) shows the engineering stress-engineering strain data for the base steel sheets.

2.2 SPR Experiments

Lap-shear sample geometry is selected based on the RSW standard, BS 1140, as standard guidelines for SPR have yet to be available. SPR joints are fabricated using an 80 kN servo-controlled electrical SPR system using standard C-type rivets with a countersunk head having a shaft diameter of 5.3 mm, rivet length of 5 mm, and hardness of 480 Hv. Rivets are made of boron steel grade 36MnB4 and coated with Zinc-Tin alloy. The chemical composition in weight % is C 0.35, Si 0.2, Mn 0.9, P 0.015, S 0.015, Cr 0.15, Cu 0.15, and B 0.0008. Two types of die, flat die and pip die, having a diameter of 9 mm and depth of 1.6 mm, are used to fabricate SPR joints. The Pip height was zero indicating pip height matches with die face.

The rivet setter and die are placed on the C-frame designed to absorb riveting force and provide accessibility to the joint from both sides. Head height (HH) is the difference between the rivet head and the top sheet's upper surface. DHH, which is desired rivet penetration into the sheets, is changed during SPR, and actual head height (AHH) is measured using the dial gauge post-riveting operation. DHH is varied at -0.4, -0.8, and 1.2 mm values, which are negative values indicating that the rivet head surface is below the upper sheet surface to enhance the total penetration of the rivet. Negative DHH is expected to achieve AHH values of either zero or slightly positive/negative values. Measuring AHH is nothing but measuring rivet head penetration, which is of paramount significance post-riveting as it controls not only the gap between the rivet head and the top sheet but also the interlock distance and bottom sheet thickness (T_b). AHH, interlock distance, and T_b are critical parameters that reliably describe the SPR joint quality (Ref 35) (refer to Fig. 2 for description). The maximum riveting force required is also captured for all the riveted joints. The cross-sectional joint quality examination is done by sectioning the joints in the center and mounting them for macroscopic examination using a Leica stereoscope. Samples are etched using 2% Nital solution post-grinding and polishing operations. The macroscopic examination includes measuring the interlock distance and T_b . The lap-shear tensile tests are performed with a 100 kN Instron 5582 tensile testing machine at 5 mm/min crosshead speed. Three samples are prepared and tested for each condition, and

the average value with standard deviation has been reported. The maximum tensile-shear load (or fracture load) is recorded during static lap-shear tests. Fracture modes are also observed to understand the failure mechanism in SPR joints. SPR setup, lap-shear test sample dimensions, rivet and die geometries are depicted in Fig. 3.

Sheet placement is an arrangement of top and bottom sheets in each stack. To study its effect, initially, CR340 was placed as the top sheet (pierced sheet facing the rivet) and CR210 as the bottom sheet (locked sheet facing the die) (referred to as the CR340-CR210 stack). This configuration uses two die designs (pip and flat) and one standard rivet. For a rivet and die combination, 15 samples were prepared (five each at three different DHHs). Hence, for one configuration, thirty samples were prepared. Secondly, sheet placement was inverted, i.e., CR210 was a top sheet, CR340 was a bottom sheet (referred to as the CR210-CR340 stack), and a similar procedure was followed to prepare the joints.

2.3 FSSW Experiments

Conventional FSSW was conducted in a three-axis FSW machine at 750, 900, and 1200 rpm at constant plunge depths of 1.2 and 1.5 mm and a plunge rate of 2 mm/min. Tools with a shoulder diameter of 8 mm, pin height of 1.3 mm, and pin diameter of 4 mm were fabricated for FSSW. Several trials were conducted to obtain successful joints; however, severe plastic deformation of the tool pin was observed without joint formation. Pinless tools were fabricated later with an 8 mm shoulder diameter for further experiments, which is closer to the rivet head diameter in SPR to minimize pin deformation. Finally, joints were formed only at 900 and 1200 rpm at 1.2 mm plunge depth and 2 mm/min plunge rate for the CR210-CR340 stack. Few trials were conducted for the CR340-CR210 stack; however, the joint formation was not repeatable. FSSW at 750 rpm was unsuccessful.

2.4 RSW Experiments

RSW joints were fabricated on a 100 kVA medium frequency direct current spot welding machine following BS1140 standard. A truncated cone-type Cu-Cr-Zr electrode cap with a 6 mm face diameter and 16 mm shank diameter was utilized. The joints were prepared for the CR340-CR210 and CR210-CR340 stacks to study the effect of sheet placement. The welding current was varied, keeping electrode force and

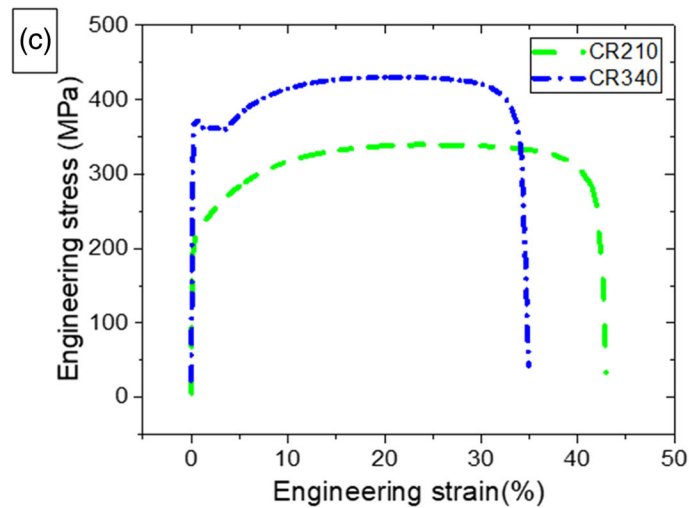
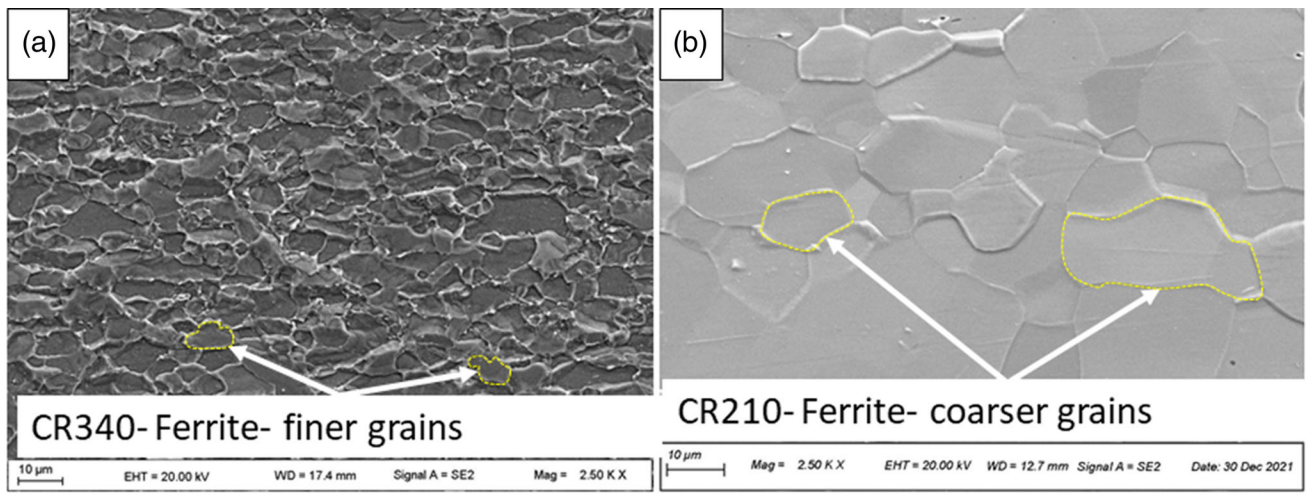


Fig. 1 Optical microstructures of (a) CR340, (b) CR210, (c) Engineering stress-Engineering strain data

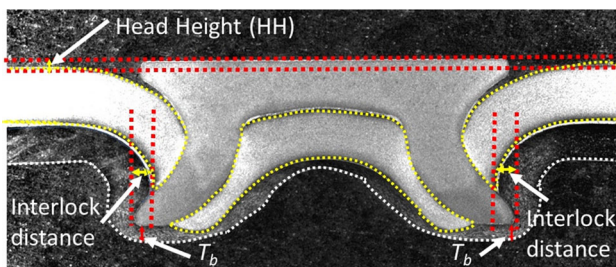


Fig. 2 Cross section of an SPR joint indicating HH, interlock distance, and T_b (AHH, DHH have the same definitions as HH)

welding time constant. The initial welding current was 5 kA and then increased with a step size of 0.5 kA to measure the nugget diameter using the standard peel test method. Welding experiments were stopped when the nugget diameter of 5.58 ± 0.32 mm was achieved, comparable with the rivet shank diameter of 5.5 ± 0.2 mm. At the optimized welding condition (Table 3), three lap-shear test samples were prepared for two different sheet placement strategies to evaluate lap-shear tensile performance.

3. Results and Discussion

3.1 SPR of CR340-CR210 Stack

Variation in AHH with DHH for pip die and flat die is shown in Fig. 4(a). It is evident that when DHH decreases to enhance the rivet penetration for both die designs, AHH decreases, indicating enhanced rivet penetration into the sheets. Positive AHH indicates that the rivet head is above the top sheet surface and closer to zero; negative AHH indicates the rivet head flushing with the top sheet or slightly indenting the top sheet required to achieve sound riveted joints. Flat die is characterized by negative AHH, while positive AHH characterizes pip die. Negative AHH indicates that rivet head penetration is more significant in the case of a flat die due to the lesser resistance provided by the thin bottom sheet to rivet deformation, and rivet legs are compressed. However, in this case, DHH of -0.4 mm did not result in joint formation as both sheets were separated post-riveting operation indicating no interlock (Fig. 5a and 6a). AHH, measured post-riveting, is always less than input DHH due to C frame deflection in the SPR machine and punch elasticity correction. The observation is independent of the die design.

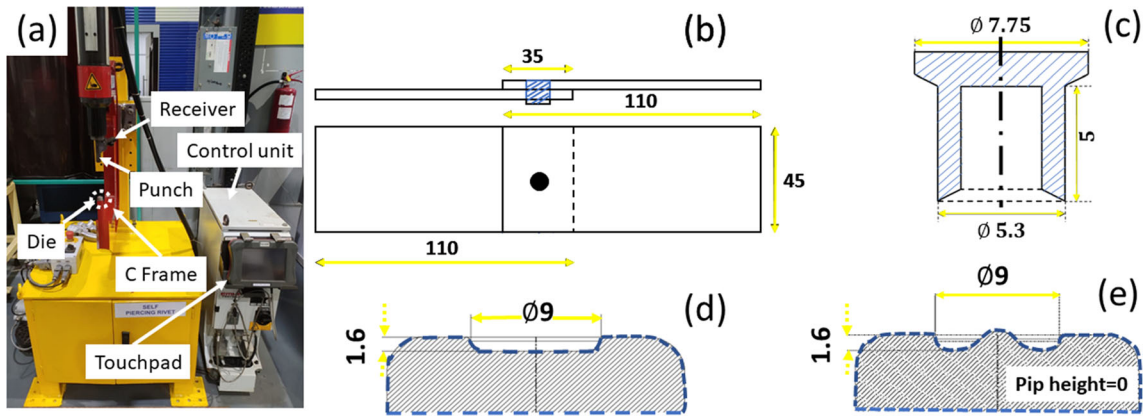


Fig. 3 (a) SPR setup (b) Lap-shear test sample dimensions (c) C type rivet, (d) Flat die, (e) Pip die (All dimensions are in mm)

Table 3 RSW parameters

Current, kA	Time, ms	Electrode pressure, kN	Squeeze time, ms	Hold time, ms	Coolant flow, L/min
7.5	200	2.8	300	83	4

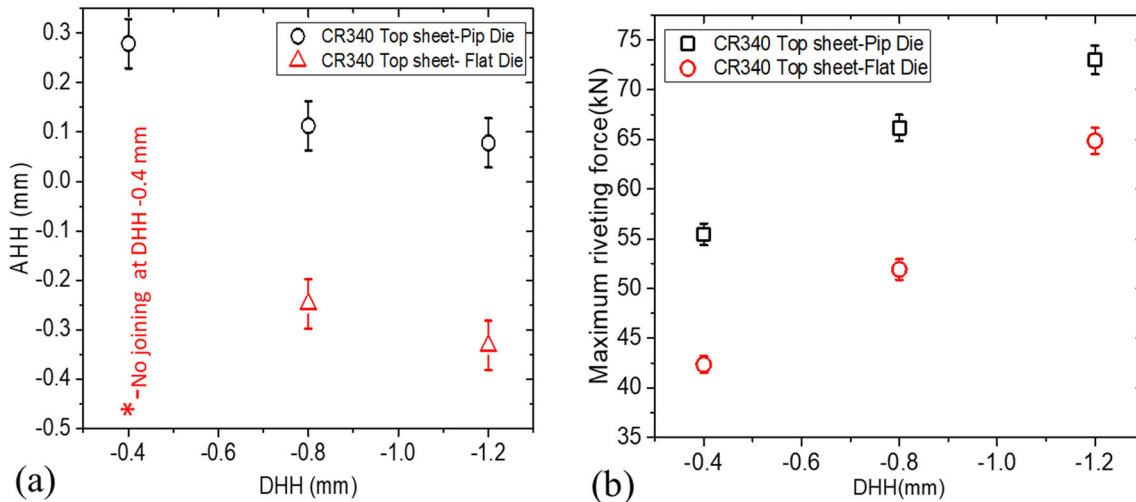


Fig. 4 Variation in (a) AHH (b) maximum riveting force for pip and flat dies

Change in maximum riveting force with DHH in the case of pip die and flat die is shown in Fig. 4(b). The maximum riveting force increases with decreasing DHH for both the dies, resulting from increased rivet penetration and enhanced strain hardening of sheets. In the case of the pip die, the maximum riveting load is higher by about 31, 27, and 13% compared to the flat die at different DHHs. The higher riveting load is due to the resistance provided by the center region in the pip die to sheet deformation resulting in enhanced strain hardening of sheets.

Variation in interlock distance with DHH for the pip die and flat die (Fig. 5a) indicates that the pip die helps achieve a higher interlock than the flat die. The interlock distance is significantly higher for the pip die. While the diameter and depth are the same for the pip die and flat die, adding a pip at the center of the die provides greater resistance to sheet deformation resulting in a higher riveting force than the flat die

design. Due to this, the bottom sheet material just above the pip reduces considerably. A significant amount of the bottom sheet material accumulates in the zone where the interlock is formed, thus enhancing the interlock distance, as shown in Fig. 6(d)-(f). In the absence of a pip in a flat die, a significant part of the bottom sheet material remained intact below the rivet instead of accumulating in the interlocking zone resulting in lower interlock distance, as shown in Fig. 6(b), (c). Xu (Ref 36) reported that the interlock distance should be greater than 0.2 mm as per industry standards for its acceptability. In the current work, joints made using a pip die produced almost twice that of the required minimum interlock value of 0.2 mm, while the flat die produced unacceptable joints as per the interlock distance requirement.

Variation in T_b for pip die and flat die is shown in Fig. 5(b). Since the rivet shaft did not penetrate the bottom sheet, T_b is slightly more in the case of a flat die as it is measured just

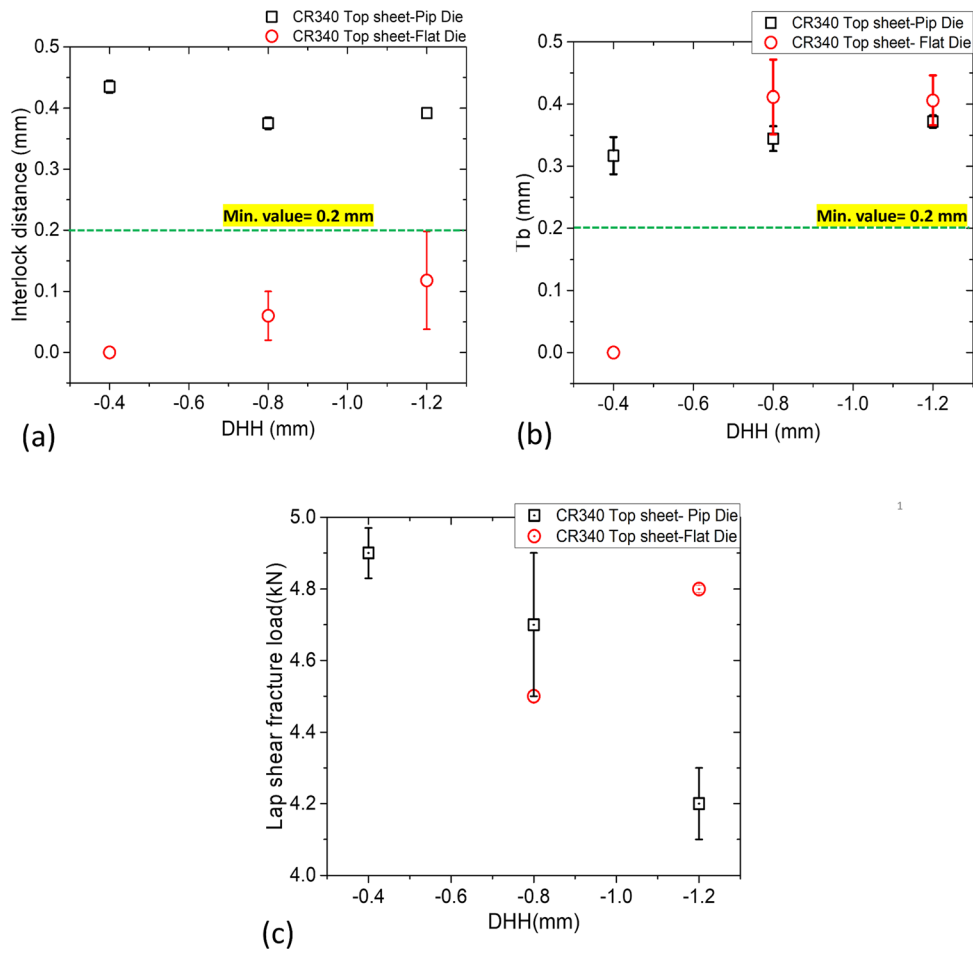


Fig. 5 Variation in (a) interlock distance (b) T_b (c) lap-shear fracture load for pip die and flat die

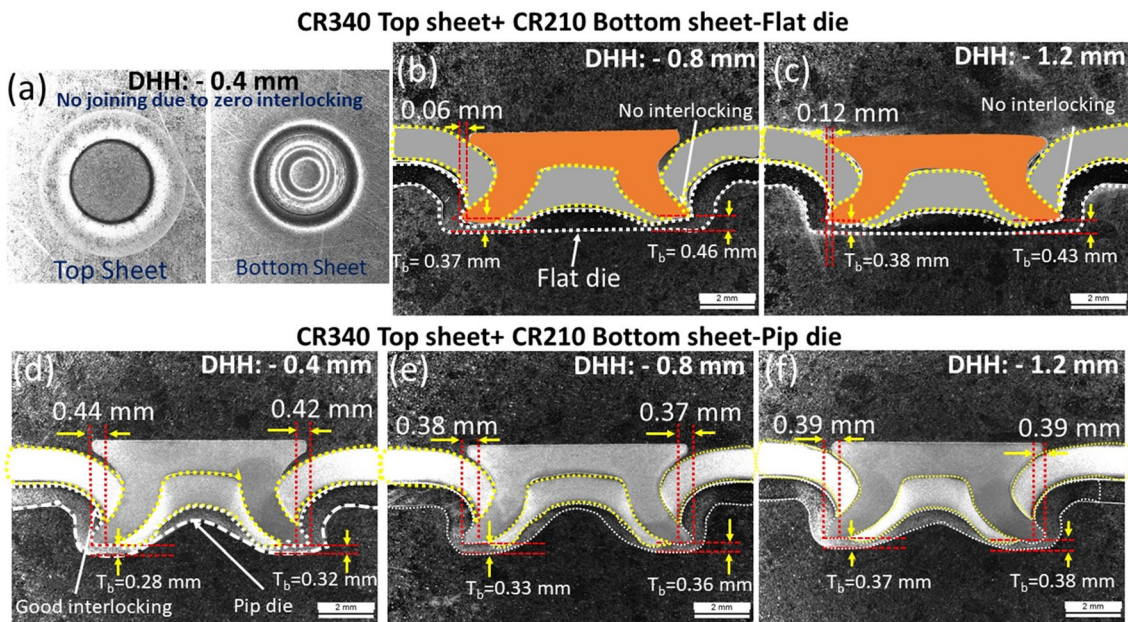


Fig. 6 Cross sections of SPR joints (CR340-CR210 stack; (a), (b), (c) for flat die; (d), (e), (f) for pip die)

below the rivet leg tip (Fig. 6b-f). Xu (Ref 36) reported that for an SPR joint to be acceptable in the industry, T_b should be at least 0.2 mm. SPR joints produced in the current work with pip die and flat die exhibit T_b above the requirement except for samples prepared at -0.4 mm DHH with the flat die at which joints could not be prepared due to no interlocking. Achieving minimum T_b is critical for joint quality in avoiding button failure due to the rivet piercing the bottom sheet completely.

Variation in lap-shear fracture load with DHH for pip die and flat die is shown in Fig. 5(c). It has been discussed that interlock distance primarily influences the tensile-shear strength of the SPR joints. For the pip die, a fracture load of 4.87 ± 0.07 kN is recorded at the maximum interlock distance of 0.43 ± 0.01 mm. With the decrease in DHH due to the reduction in interlock distance, the lap-shear fracture load reduces to 4.24 ± 0.10 kN. For the flat die, a fracture load of 4.81 ± 0.01 kN was recorded at the maximum interlock distance of 0.12 ± 0.08 mm. Gross button failure was observed for most of the joints, while the rivet was pulled out from the weaker, thinner bottom sheet, as shown in Fig. 7(a)-(c) and (e). During tensile-shear loading, the rivet leg tip, while bending, pierced the button, and failure took place in the CR210 bottom sheet. However, for the flat die DHH -0.8 mm sample, the rivet was pulled out from the bottom sheet without significant damage to the button, as shown in Fig. 7(d). As evident in Fig. 6(b), the interlock distance obtained for the joint is the lowest in this case, and there is a gap between the rivet head and the top sheet resulting in easy separation of the riveted top sheet and the bottom sheet.

3.2 SPR of CR210-CR340 Stack

This section discusses results derived when CR210 (low strength, thin sheet) was kept as the top sheet and CR340 (high strength, thick sheet) as the bottom sheet. With decreasing DHH, AHH decreases, indicating a reduction in the gap between the rivet head and the top sheet (Fig. 8a). In the case of the flat die, better penetration is observed at all DHH levels compared to the pip die. A similar trend was observed for the CR340-CR210 stack (discussed in Sect. 3.1). It can be interpreted that having a thicker sheet on the die side (as the bottom sheet) in the case of the pip die improves rivet flushness (Fig. 4a and 8a).

Variation in riveting force with DHH (Fig. 8b) for CR210-CR340 stack is like CR340-CR210 stack (Fig. 4b). It can be noted that (i) the maximum riveting force required increases with a decrease in DHH, which is the consequence of increased

rivet penetration and enhanced strain hardening of sheets, and (ii) an increased riveting force is required in the case of pip die as compared to flat die which is due to enhanced strain hardening of sheets provided by pip during deformation.

Variation in interlock distance, T_b , and lap-shear fracture load with DHH for CR210-CR340 stack presented in Fig. 9(a)-(c) and demonstrated using cross-sectional images (Fig. 10a-f) indicates.

- (i) Insignificant effect of DHH as these outputs vary within a small range.
- (ii) Interlock distance is slightly higher in the case of pip die (Fig. 9a), which coincides with the observation when CR210 is kept as a bottom sheet (Fig. 5a).
- (iii) Interlock distance for both the dies is significantly higher than the minimum acceptable value of 0.2 mm suggested in Xu (Ref 36).
- (iv) Joints made by pip die do show improved T_b by about 58-100% as compared to flat die at different DHH values (Fig. 9b), and it is higher than 0.2 mm minimum standard requirement suggested in Xu (Ref 36). Joints made by flat die do not satisfy the requirement.
- (v) Joints made by flat die exhibit higher load-bearing ability as observed from lap-shear fracture load data (Fig. 9c), though the improvement is only within 0.1 to 0.3 kN.

Fracture modes of SPR joints for the CR210-CR340 stack (Fig. 11) differed from the CR340-CR210 stack. However, in this case, too, die design was not a prominent factor influencing the fracture mode. Here, the rivet is locked in the CR340 bottom sheet (Fig. 11a-f), confirming a better interlock with the thicker steel sheet on the die side. A more robust interlock resulted in partial bending of the rivet, which led to exerting compressive load by the rivet head. Therefore, severe stress concentration on the weaker, thinner CR210 top sheet just below the rivet head caused partial/complete tearing of the sheet. Lap-shear fracture load did not differ much (Fig. 9c) as all the samples failed with similar fracture modes irrespective of die design.

3.3 Influence of Sheet Placement on the SPR Joint Performance

Figure 12 shows the summary of the effect of the placement of CR210 and CR340 sheets concerning die design on the SPR outputs. The following is notable results.

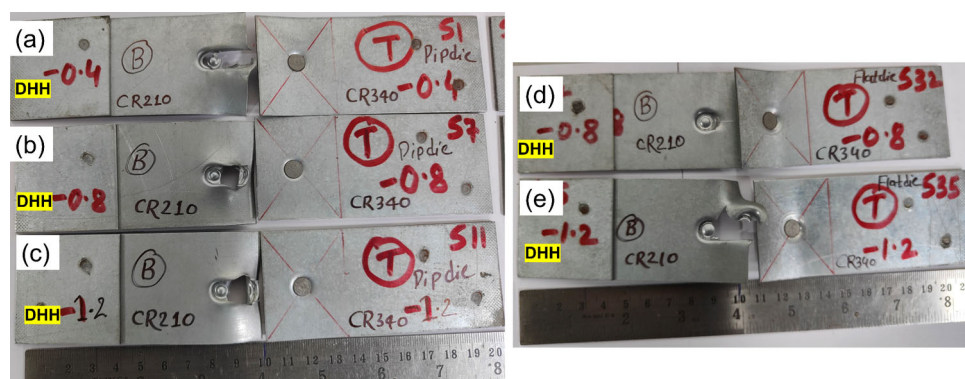


Fig. 7 Fracture modes during lap-shear tensile tests [CR340-CR210 stack; (a, b, c) pip die; (d, e) flat die]

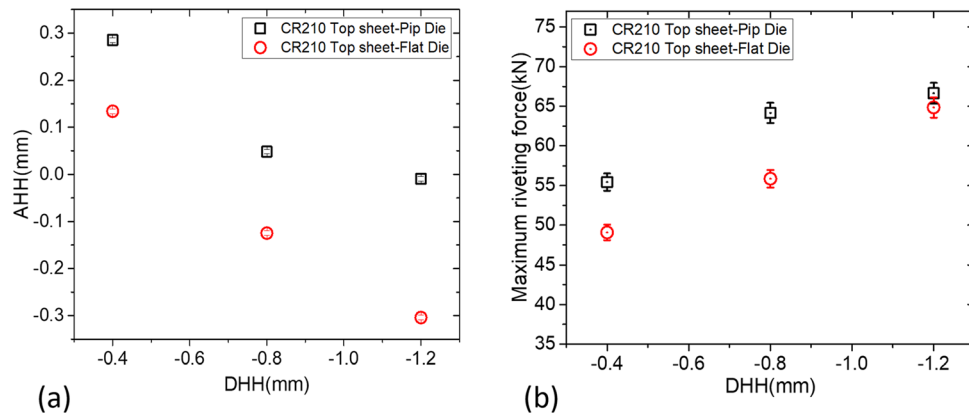


Fig. 8 Variation in (a) AHH (b) riveting force with DHH for pip and flat dies

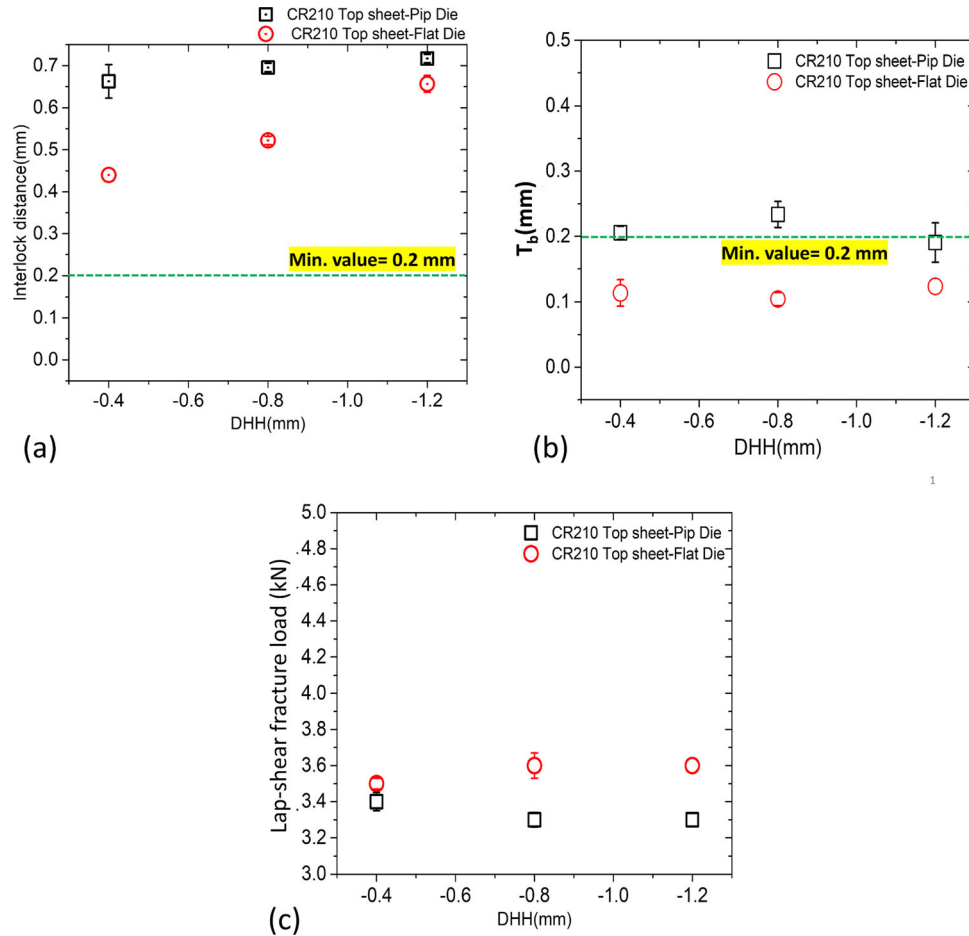


Fig. 9 Variation in (a) interlock distance (b) T_b (c) lap-shear fracture load for pip die and flat die

In the case of pip die,

- The effect of CR210 as the top sheet is to improve AHH as it is closer to zero in the case of DHH of -0.8 and 1.2 mm (Fig. 12a). In the case of -0.4 mm DHH, placement of the sheet has negligible effect.
- The maximum riveting force required is reduced for the CR210-CR340 stack, and a significant difference of about 10 kN is witnessed with a decrease in DHH compared to

that obtained in the case of the CR340-CR210 stack (Fig. 12b).

- Interlock is better in the case of the CR210-CR340 stack in all the DHH cases chosen (Fig. 12c). About 40 - 50% improvement is observed for the CR210-CR340 stack compared to the CR340-CR210 stack.
- T_b is better for the CR340-CR210 stack due to larger AHH indicating lesser rivet penetration (Fig. 12d).

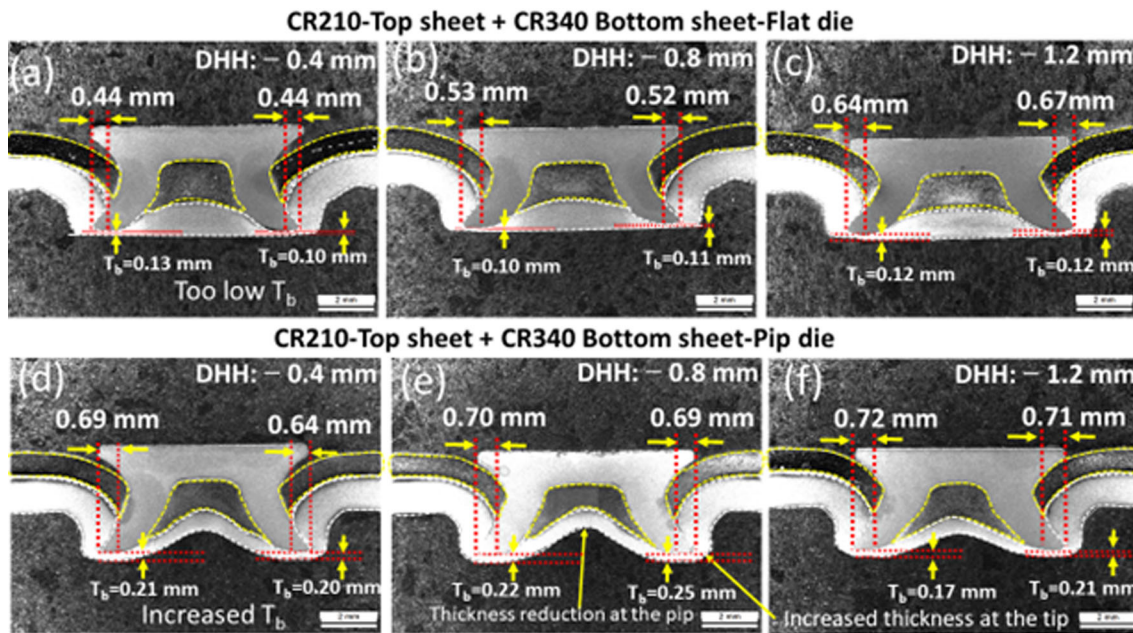


Fig. 10 Cross-sectional macrographs of SPR joints at DHH of -0.4 , -0.8 , and -1.2 mm (CR210-CR340 stack; (a), (b), (c) for flat die; (d), (e), (f) for pip die)

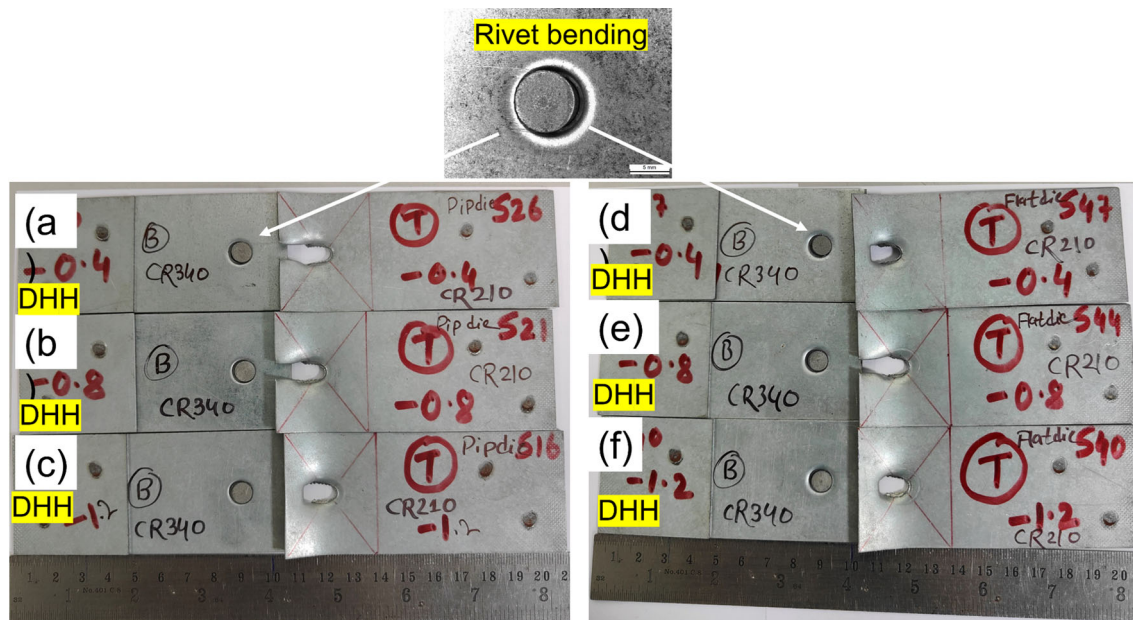


Fig. 11 Fracture modes during lap-shear tests [CR210- CR340 stack; (a), (b), (c) pip die; (c), (d), (e) flat die]

- Lap-shear fracture load has significantly reduced (about 35-45%) for the CR210-CR340 stack. However, the interlock is better (Fig. 12e). This reduction is mainly due to tearing the thinner top sheet from the rivet-trapped thicker bottom sheet requiring lesser fracture load as presented in fracture mode (Fig. 11).

In the case of a flat die,

- The effect of CR210 as the top sheet is to improve AHH as it is closer to zero in the case of -0.8 and -1.2 mm DHH (Fig. 12a). While the joint is not at all formed at 0.4 mm DHH in the case of CR340 as a top sheet, the

placement of sheets at -1.2 mm DHH results in deeper indentation independent of top sheet quality. It may affect the dynamic performance of the joints due to severe stress concentration.

- CR340, as the top sheet, produced joint at lesser riveting force; however, the case with CR210 as the top sheet, performed equally when DHH is decreased (Fig. 12b).
- CR210, as the top sheet, is better when the interlock distance is compared, and when it is kept as the bottom sheet, there is a significant reduction in interlocking ability (Fig. 12c).
- Like in the pip die, in the case of the flat die, T_b is better for the CR340-CR210 stack (Fig. 12d), indicating higher rivet penetration as presented in the AHH variation.

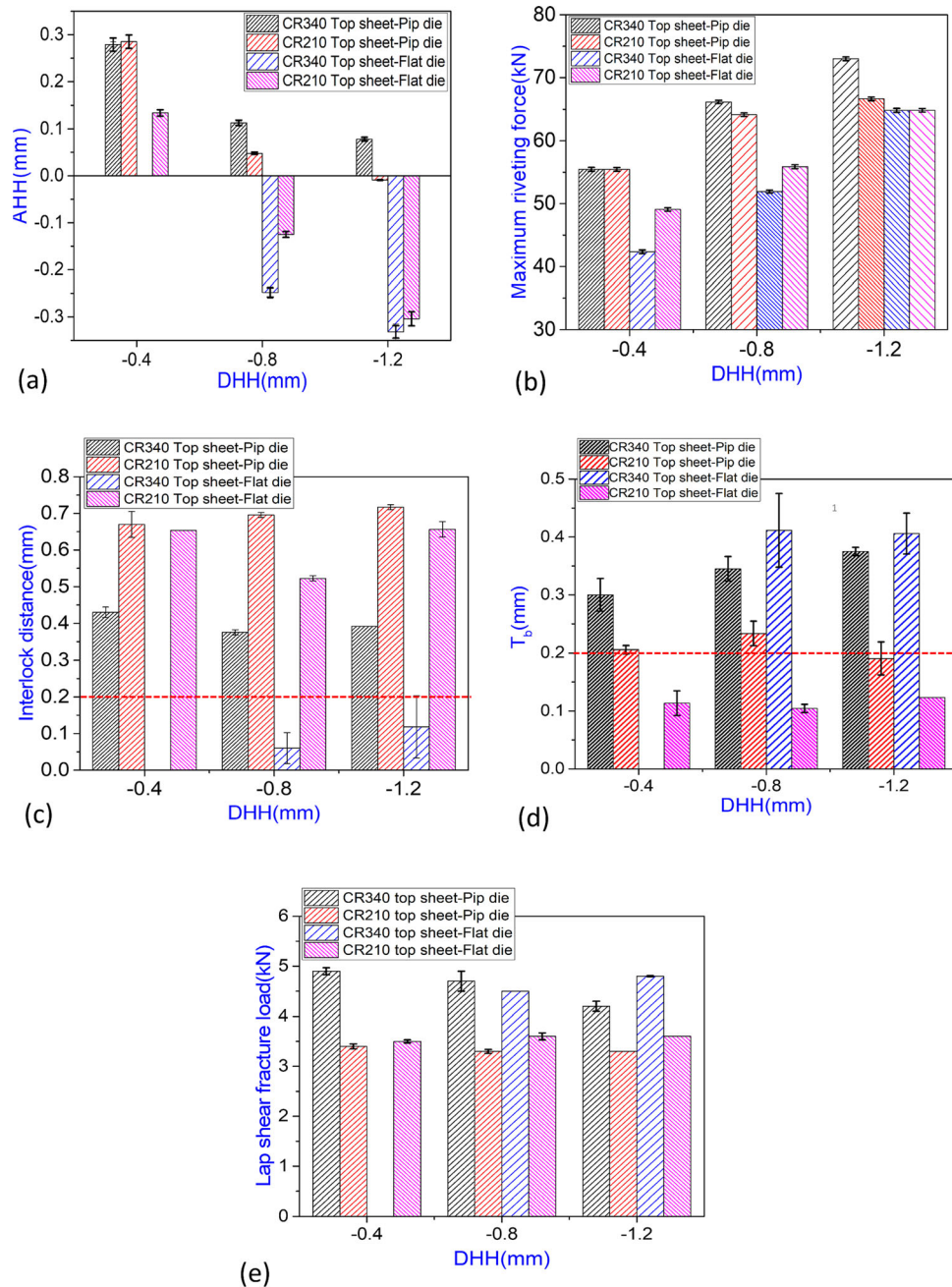


Fig. 12 Consolidated results showing the effect of placement of sheets on joint performance (No joining occurred at DHH -0.4 mm pip die CR340-CR210 stack)

- Like the pip die, when the flat die is used, placing CR210 as the top sheet has reduced the lap-shear fracture load (Fig. 12e) due to fracture mode, i.e., tearing of CR210 top sheet from rivet trapped in the bottom CR340 sheet (Fig. 11).

To summarize the effect of placement of sheets during SPR, placing a CR210 (weaker, thinner) sheet as a top sheet, i.e., facing the punch, would be beneficial if riveting force and interlock distance are referred to. This can be inferred for both pip and flat dies. However, if T_b and fracture load in the lap-shear test are considered, placing the CR340 (stronger, thicker) sheet at the top would be acceptable. The observation partially coincides with Ma et al. (Ref 37) work, in which it is suggested to have AZ31B (weaker, thinner) as the top sheet and AA6061-

T6 (stronger, thicker) as the bottom sheet. Similarly, Li et al. (Ref 38) suggested thicker material as the bottom sheet to exhibit better rivetability, which coincides partially with the present findings that the thinner sheet (CR210) should be kept as the top sheet for better interlock distance and lower rivet force. However, Li et al. (Ref 38) worked on aluminum alloys to make such conclusions.

Recently, Xie et al. (Ref 33) proposed design guidelines for SPR joints made of galvanized steel sheets in which it is evaluated that shear capacity is between 4 and 8 kN when bottom to top sheet thickness ratio (t_2/t_1) is between 1 and 1.5. In the present work, CR340 as the top sheet produced SPR joints within the range (refer Fig. 12c) for both the dies and the case of CR210 as the top sheet has not satisfied this. This also

coincides with the inference from the present work when lap-shear fracture load is referred to for characterizing SPR joints.

Xie et al. (Ref 33) have also proposed shear capacity models for SPR joints made of galvanized steel sheets after careful analyses and examination of failure modes of screw connections as per AISI S100-16 and SPR joints as per Haque et al. (Ref 39). The models are,

$$\text{For } \frac{t_2}{t_1} \geq 1.5, F_s = \alpha_2 t_1 d_w \sigma_{YU} \quad (\text{Eq 1})$$

$$\text{For } \frac{t_2}{t_1} = 1, F_s = \alpha_1 t_2 (L d_s)^{0.5} \sigma_{YL} \quad (\text{Eq 2})$$

where t_1 and t_2 are the thicknesses of the top sheet and bottom sheet, respectively, α_1 ($=3.52$) and α_2 ($=2.58$) are calculated coefficients, d_s is the diameter of the rivet shank ($=5.3$ mm), d_w is the diameter of the rivet head ($=7.75$ mm), σ_{YL} and σ_{YU} are the yield strengths of bottom and top sheets, respectively, F_s is the shear fracture load. L is the actual rivet length ($=5$ mm) used in the present calculations and not the optimal value proposed in Xie et al. (Ref 33).

F_s calculated from the models (Eq 1 and 2) and comparison with current experimental data is presented in Table 4. A good agreement is seen for the CR210-CR340 stack. Equation 2 underpredicts F_s observed in SPR experiments for the CR340-CR210 stack.

3.4 Static Tensile-Shear Performance

The lap-shear test performance of SPR, RSW, and FSSW joints is compared in Fig. 13 and 14 for their load evolution and fracture modes, respectively. RSW joints exhibit a higher

load of about 5.69 ± 0.06 kN and 5.74 ± 0.04 kN when CR340 is kept as the top sheet (Fig. 13a) and the bottom sheet (Fig. 13b), respectively. The sheet placement does not influence the fracture load significantly. Load-bearing capacity of SPR joints reached up to 4.87 ± 0.07 kN, about 86% of RSW, in a pip die case. The previous study (Ref 25) also observed similar static-tensile performance for RSW and SPR dissimilar steel stacks. In some SPR cases (curves distinctly shown in Fig. 13a), large local elongation is witnessed, which is not seen in RSW. FSSW is not possible with CR340 as the top sheet.

When CR210 is kept as the top sheet (Fig. 13b), SPR joints show moderate performance with a maximum load reaching 3.6 ± 0.03 kN (about 63% of RSW joints). However, significant local elongation is seen. FSSW joints made at 900 rpm exhibited a maximum fracture load of 4.93 ± 0.05 kN, equivalent to about 86% of those obtained in RSW, and 3.48 ± 0.07 kN for joints made at 1200 rpm, which is about 60% of those obtained in RSW (Fig. 13b). FSSW joints performed at par with SPR cases (Fig. 13b).

While RSW joints failed by the desirable button pullout along with tearing of thinner, weaker CR210 sheet (Fig. 14a, b), which is consistently found in all trials independent of sheet placement, FSSW joints failed by interface failure at 1200 rpm and pullout failure at 900 rpm (Fig. 14c, d). As a result, the 900-rpm case tolerated a larger maximum load and larger local elongation than the 1200 rpm case (Fig. 13b). Fracture modes of SPR joints are discussed elaborately in the earlier sections. Asati et al. (Ref 25) reported that the lap-shear performance of RSW joints for steel-steel thin gauge stack was superior to SPR joints. They correlated lap-shear fracture load to nugget diameter. As evident from Fig. 13(a), (b), energy absorption

Table 4 Calculation of F_s of SPR joint from available models and experiments

Top sheet	Bottom sheet	t_2/t_1	Model used	F_s from models	F_s from experiments
CR210	CR340	1.5	Equation 1	3.34 kN	3.25 to 3.7 kN (refer to Fig. 8c, 11e)
CR340	CR210	0.67	Equation 2 *	3.04 kN	4.2 to 4.9 kN (refer Fig. 4c, 11e)

*Equation 2 is used though it is meant for $\frac{t_2}{t_1} = 1$, and no model is available for $\frac{t_2}{t_1} < 1$

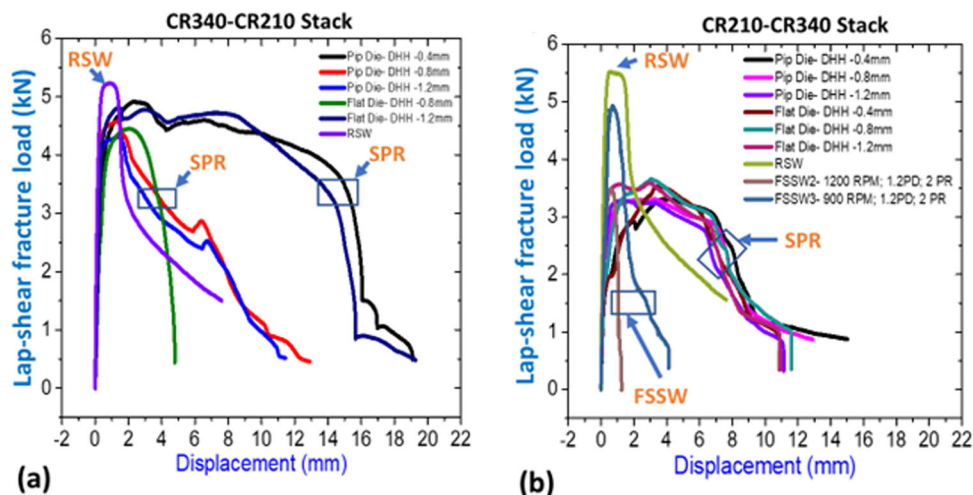


Fig. 13 Comparison of lap-shear test performance of SPR, RSW, FSSW joints, (a) CR340-CR210 stack, (b) CR210-CR340 stack

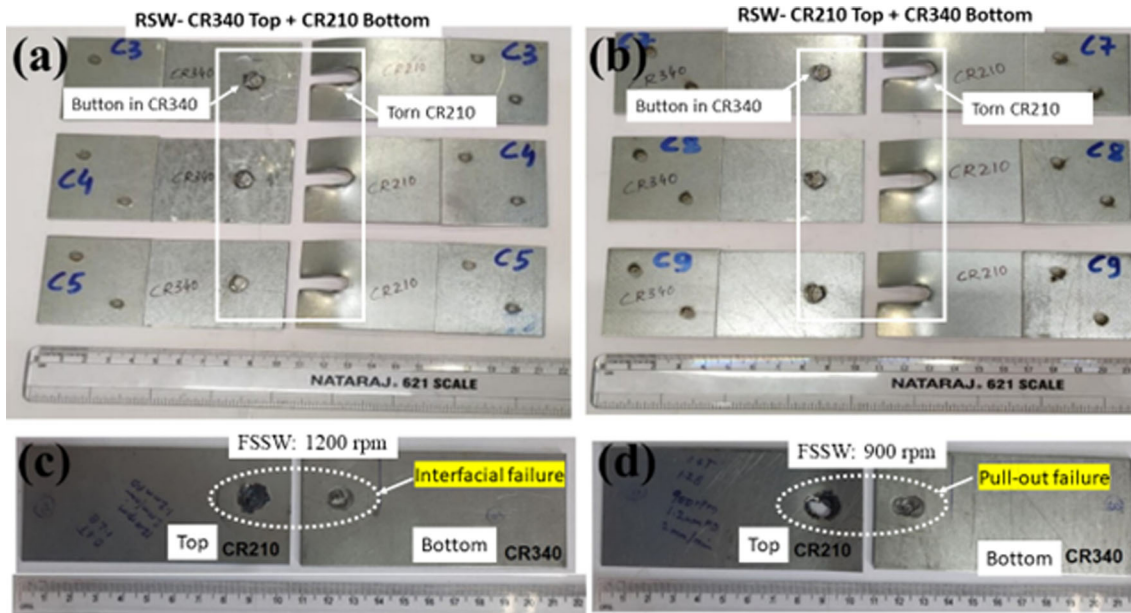


Fig. 14 Fracture modes during lap-shear tests of RSW and FSSW joints, (a) RSW: CR340-CR210 stack, (b) RSW: CR210- CR340 stack, (c) FSSW: 1200 rpm, 1.2 mm PD, 2 mm/min plunge speed; (d) FSSW: 900 rpm, 1.2 mm PD, 2 mm/min plunge speed (FSSW is done with CR210 on top)

at fracture is consistently higher for SPR joints, which could be due to larger displacement at fracture than RSW and FSSW joints. In addition, the interlock formed in SPR joints can sustain the load for a longer duration compared to RSW joints, even beyond the point of maximum load (Ref 40). Due to similar fracture modes (Fig. 14a, b), sheet placement has an insignificant effect on the tensile-shear fracture load of RSW joints. The thinner, weaker steel sheet shall be considered for dissimilar stacks while deciding the mechanical performance requirement.

In the case of SPR, the tensile-shear fracture load was observed to be higher for the CR340 + CR210 stack than the CR210 + CR340 stack. This can be attributed to the different failure modes discussed earlier. For the CR210 + CR340 stack, partial pullout of the rivet led to some slight bending and the partial/complete tearing of the thinner, weaker CR210 sheet. In contrast, for the CR340 + CR210 stack, complete tearing of the thinner, weaker CR210 sheet failed the joint with no damage observed in the rivet and the top sheet (thicker and harder CR340). This contributed to a higher tensile-shear fracture load compared to the CR210 + CR340 stack. The results agree with Han et al.'s findings (Ref 40, 41).

In RSW, the best sheet placement would be CR210 on top of CR340, as it showed a slightly higher fracture load of 5.74 kN. In SPR, considering the cross-sectional quality and the lap-shear performance, CR340, on top of CR210, made using a pip die with DHH of -0.4 mm, can be considered the best choice. In FSSW, the best choice is 900 rpm, considering the higher tensile-shear fracture load and the desirable pullout failure mode. Out of RSW, SPR, and FSSW, RSW performed superior in terms of fracture load, followed by the equally good performance of SPR and FSSW. Considering displacement at fracture, SPR performance was superior to RSW and FSSW, and RSW was superior to FSSW.

4. Conclusions

SPR of CR210 and CR340 galvanized steel sheets of dissimilar thicknesses and strengths are investigated to understand the effect of die design and sheet placement on the joint quality. The following conclusions are drawn from the results obtained.

- Flat die improved rivet penetration irrespective of sheet placement, providing better rivet flushness with the top sheet, which deters corrosion.
- Maximum riveting force in the case of pip die is higher irrespective of sheet placement indicating better rivetability.
- Pip die improved interlock by 50-80% compared to flat die, irrespective of the sheet placement. For dissimilar stacks, a thicker sheet on the die side increased interlock distance with a simultaneous reduction in T_b due to improved interlock. However, in the pip die, T_b is larger than the required minimum of 0.2 mm.
- For SPR joints, tensile-shear load and fracture modes are influenced primarily by sheet placement, whereas die design has only a marginal influence. For the thicker bottom sheet (CR340), 44% lower tensile-shear load was recorded for both die designs primarily due to fracture of lower strength, thinner CR210 top sheet. For RSW joints, sheet placement is insignificant vis-à-vis tensile-shear performance.
- Among SPR, RSW, and FSSW joints, RSW joints exhibited the maximum fracture load of 5.74 ± 0.04 kN compared to 4.87 ± 0.07 kN for SPR joints of CR340-CR210 stack with a pip die and 4.93 ± 0.05 kN for FSSW joints of CR210-CR340 stack for 900 rpm.

- SPR joints' fracture mode changed with sheet placement, irrespective of die design. For the CR340-CR210 stack, most of the joints failed with a complete fracture of the CR210 sheet. In contrast, the CR210-CR340 stack failed with partial/complete tearing of CR210 caused by bending of the rivet. RSW joints failed in pullout mode with complete tearing of CR210 sheet irrespective of sheet placement. FSSW joints failed by interface failure at 1200 rpm and pullout failure at 900 rpm.

Author contributions

All authors contributed to the study's conception and design. Material preparation, data collection, and analysis were performed by (Brajesh Asati), (R Ganesh Narayanan) and (Nikhil Shajan). The first draft of the manuscript was written by (Brajesh Asati), and all authors commented on previous versions. All authors read and approved the final manuscript.

References

1. E. E. Agency—EEA, Monitoring CO₂ emissions from passenger cars and vans in 2018, ed: EEA Luxembourg, 2020. <https://www.eea.europa.eu/publications/co2-emissions-from-cars-and-vans-2018>
2. K. Matsuyama, Trend of Automobile Vehicles and the Joining Technologies, *Weld. World*, 2007, **51**(3), p 50–60. <https://doi.org/10.1007/BF03266560>
3. S. Singh, O. Hahn, F. Du, and G. Zhang, Lightweight Design Through Optimised Joining Technology, *Weld. World*, 2002, **46**(9), p 10–18. <https://doi.org/10.1007/BF03377344>
4. G. Weber and S. Göklü, Resistance Spot Welding of Uncoated and Zinc Coated Advanced High-Strength Steels (AHSS)—Weldability and Process Reliability—Influence of Welding Parameters, *Weld. World*, 2006, **50**(3), p 3–12. <https://doi.org/10.1007/BF03263428>
5. R. Ashiri, M.A. Haque, C.-W. Ji, H.R. Salimijazi, and Y.-D. Park, Supercritical Area and Critical Nugget Diameter for Liquid Metal Embrittlement of Zn-Coated Twinning Induced Plasticity Steels, *Scr. Mater.*, 2015, **109**, p 6–10. <https://doi.org/10.1016/j.scriptamat.2015.07.006>
6. R. Ashiri, H. Mostaan, and Y.-D. Park, A Phenomenological Study of Weld Discontinuities and Defects in Resistance Spot Welding of Advanced High Strength TRIP Steel, *Metall. Mater. Trans. A*, 2018, **49**(12), p 6161–6172. <https://doi.org/10.1007/s11661-018-4900-0>
7. S. Salimi-Beni, M. Atapour, M.R. Salmani, and R. Ashiri, Resistance Spot Welding Metallurgy of Thin Sheets of Zinc-Coated Interstitial-Free Steel, *Metall. Mater. Trans. A*, 2019, **50**(5), p 2218–2234. <https://doi.org/10.1007/s11661-019-05146-8>
8. R. Ashiri, S. Marashi, and Y. Park, Weld Processing and Mechanical Responses of 1-GPa TRIP Steel Resistance Spot Welds, *Welding J.*, 2018, **97**, p 157–169
9. J.W. Kim, S. Murugan, J.-H. Yoo, R. Ashiri, and Y.-D. Park, Enhancing Nugget Size and Weldable Current Range of Ultra-High-Strength Steel using Multi-Pulse Resistance Spot Welding, *Sci. Technol. Weld. Joining*, 2020, **25**(3), p 235–242. <https://doi.org/10.10080/13621718.2019.1680483>
10. G. Meschut, O. Hahn, V. Janzen, and T. Olfemann, Innovative Joining Technologies for Multi-Material Structures, *Weld. World*, 2014, **58**(1), p 65–75. <https://doi.org/10.1007/s40194-013-0098-3>
11. Y. Huang, J. Wang, L. Wan, X. Meng, H. Liu, and H. Li, Self-Riveting Friction Stir Lap Welding of Aluminum Alloy to Steel, *Mater. Lett.*, 2016, **185**, p 181–184. <https://doi.org/10.1016/j.matlet.2016.08.102>
12. Y. Huang, T. Huang, L. Wan, X. Meng, and L. Zhou, Material Flow and Mechanical Properties of Aluminum-To-Steel Self-Riveting Friction Stir Lap Joints, *J. Mater. Process. Technol.*, 2019, **263**, p 129–137. <https://doi.org/10.1016/j.jmatprotec.2018.08.011>

13. Y. Huang, Z. Lv, L. Wan, J. Shen, and J.F. dos Santos, A New Method of Hybrid Friction Stir Welding Assisted by Friction Surfacing for Joining Dissimilar Ti/Al Alloy, *Mater. Lett.*, 2017, **207**, p 172–175. <https://doi.org/10.1016/j.matlet.2017.07.081>
14. K.-I. Mori and Y. Abe, A Review on Mechanical Joining of Aluminium and High Strength Steel Sheets by Plastic Deformation, *Int. J. Lightweight Mater. Manuf.*, 2018, **1**(1), p 1–11. <https://doi.org/10.1016/j.ijlmm.2018.02.002>
15. X. Hes, I. Pearson, and K. Young, Self-Pierce Riveting for Sheet Materials: State of the Art, *J. Mater. Process. Technol.*, 2008, **1**(3), p 27–36. <https://doi.org/10.1016/j.jmatprotec.2007.10.071>
16. B. Asati, N. Shajan, and K.S. Arora, Effect of Process Parameters on Joint Performance in Self-Piercing Riveted Dissimilar Automotive Steel Joints, *Mater. Today: Proc.*, 2022 <https://doi.org/10.1016/j.matpr.2022.03.658>
17. J.-H. Deng, F. Lyu, R.-M. Chen, and Z.-S. Fan, Influence of Die Geometry on Self-Piercing Riveting of Aluminum Alloy AA6061-T6 to Mild Steel SPFC340 Sheets, *Advances in Manufacturing*, 2019, **7**(2), p 209–220. <https://doi.org/10.1007/s40436-019-00250-9>
18. L. Han and A. Chrysanthou, Evaluation of Quality and Behaviour of Self-Piercing Riveted Aluminium to High Strength Low Alloy Sheets with Different Surface Coatings, *Mater. Des.*, 2008, **29**(2), p 458–468. <https://doi.org/10.1016/j.matdes.2006.12.020>
19. N. Karathanasopoulos, K.S. Pandya, and D. Mohr, An Experimental and Numerical Investigation of the Role of Rivet and Die Design on the Self-Piercing Riveting Joint Characteristics of Aluminum and Steel Sheets, *J. Manuf. Processes*, 2021, **69**, p 290–302. <https://doi.org/10.1016/j.jmapro.2021.07.049>
20. K. Mori, Y. Abe, and T. Kato, Self-Pierce Riveting of Multiple Steel and Aluminium Alloy Sheets, *J. Mater. Process. Technol.*, 2014, **214**(10), p 2002–2008. <https://doi.org/10.1016/j.jmatprotec.2013.09.007>
21. I. Papadimitriou, P. Efthymiadis, H. Kotadia, I. Sohn, and S. Sridhar, Joining TWIP to TWIP and TWIP to aluminium: A Comparative Study Between Joining Processes, Joint Properties and Mechanical Performance, *J. Manuf. Processes*, 2017, **30**, p 195–207. <https://doi.org/10.1016/j.jmapro.2017.09.012>
22. Z. Du, L. Duan, L. Jing, A. Cheng, and Z. He, Numerical Simulation and Parametric Study on Self-Piercing Riveting Process of Aluminium–Steel Hybrid Sheets, *Thin-Walled Struct.*, 2021, **164**, 107872. <https://doi.org/10.1016/j.tws.2021.107872>
23. Z. Du, B. Wei, Z. He, A. Cheng, L. Duan, and G. Zhang, Experimental and Numerical Investigations of Aluminium–Steel Self-Piercing Riveted Joints Under Quasi-Static and Dynamic Loadings, *Thin-Walled Struct.*, 2021, **169**, 108277. <https://doi.org/10.1016/j.tws.2021.108277>
24. C.S. Chung and H.K. Kim, Fatigue Strength of Self-Piercing Riveted Joints in Lap-Shear Specimens of Aluminium and Steel Sheets, *Fatigue Fract. Eng. Mater. Struct.*, 2016, **39**(9), p 1105–1114. <https://doi.org/10.1111/ffe.12419>
25. B. Asati, N. Shajan, V.T. Akhil-Kishore, K.S. Arora, and R.G. Narayanan, A Comparative Investigation on Self-Piercing Riveting and Resistance Spot Welding of Automotive Grade Dissimilar Galvanized Steel Sheets, *Int. J. Adv. Manuf. Technol.*, 2022 <https://doi.org/10.1007/s00170-022-10226-y>
26. V.T. Akhil-Kishore, B. Asati, N. Shajan, and K.S. Arora, Performance Evaluation of Self-Piercing Riveted and Resistance Spot Welded Dissimilar Steel Joints, *ARAI J. Mobi. Tech.*, 2021, **1**(1), p 34–42. <https://doi.org/10.37285/ajmt.1.0.5>
27. Y. Ma, M. Lou, Y. Li, and Z. Lin, Effect of Rivet and Die on Self-Piercing Rivetability of AA6061-T6 and Mild Steel CR4 of Different Gauges, *J. Mater. Process. Technol.*, 2018, **251**, p 282–294. <https://doi.org/10.1016/j.jmatprotec.2017.08.020>
28. Y. Liu, H. Li, H. Zhao, and X. Liu, Effects of the Die Parameters on the Self-Piercing Riveting Process, *Int. J. Adv. Manuf. Technol.*, 2019, **105**(7), p 3353–3368. <https://doi.org/10.1007/s00170-019-04567-4>
29. Z. Rao, L. Ou, Y. Wang, and P.-C. Wang, A Self-Piercing-Through Riveting Method for Joining of Discontinuous Carbon Fiber Reinforced Nylon 6 Composite, *Compos. Struct.*, 2020, **237**, p 111841. <https://doi.org/10.1016/j.compstruct.2019.111841>
30. S. Gupta, S. Das, R.G. Narayanan, and B. Asati, Friction Stir Spot Welding of Dissimilar Quality Galvanized Steel Sheets Meant FOR Automotive Applications Using a Consumable Sheet, *Inst. Mech. Eng. J. Process Mech. Eng Proc*, 2022 <https://doi.org/10.1177/09544089221117935>

31. H.S. Bang et al., Mechanical Properties of Dissimilar a356/saph440 Lap Joints by the Friction Stir Spot Welding and Self-Piercing Riveting, *Strength Mater.*, 2018, **50**(1), p 63–71. <https://doi.org/10.1007/s11223-018-9943-3>
32. M. Lou, Y. Li, Y. Wang, B. Wang, and X. Lai, Influence of Resistance Heating on Self-Piercing Riveted Dissimilar Joints of AA6061-T6 and Galvanized DP590, *J. Mater. Process. Technol.*, 2014, **214**(10), p 2119–2126. <https://doi.org/10.1016/j.jmatprotec.2014.03.006>
33. Z. Xie, A. Zhang, W. Yan, Y. Zhang, T. Mu, and C. Yu, Study on Shear Performance and Calculation Method for Self-Pierce Riveted Joints in Galvanized Steel Sheet, *Thin-Walled Struct.*, 2021, **161**, 107490. <https://doi.org/10.1016/j.tws.2021.107490>
34. D. Li, G. Williams, L. Han, and M. Shergold, Influence of Stack Orientations on the Static Strengths of SPR Joints, in *3rd Annual International Conference on Advanced Material Engineering (AME 2017)*, 2017: Atlantis Press, pp 329–336. <https://doi.org/10.2991/ame-17.2017.55>
35. R. Haque, Quality of Self-Piercing Riveting (SPR) Joints from Cross-Sectional Perspective: A Review, *Arch. Civ. Mech. Eng.*, 2018, **18**(1), p 83–93. <https://doi.org/10.1016/j.acme.2017.06.003>
36. Y. Xu, Effects of Factors on Physical Attributes of Self-Piercing Riveted Joints, *Sci. Technol. Weld. Joining*, 2006, **11**(6), p 666–671. <https://doi.org/10.1179/174329306X131866>
37. Y. Ma, S. Niu, H. Shan, Y. Li, and N. Ma, Impact of Stack Orientation on Self-Piercing Riveted and Friction Self-Piercing Riveted Aluminum Alloy and Magnesium Alloy Joints, *Automot. Innovat.*, 2020, **3**(3), p 242–249. <https://doi.org/10.1007/s42154-020-00108-y>
38. D. Li, A. Chrysanthou, I. Patel, and G. Williams, Self-Piercing Riveting—A Review, *Int. J. Adv. Manuf. Technol.*, 2017, **92**(5), p 1777–1824. <https://doi.org/10.1007/s00170-017-0156-x>
39. R. Haque, N.S. Williams, S.E. Blacket, and Y. Durandet, A Simple but Effective Model for Characterizing SPR Joints in Steel Sheet, *J. Mater. Process. Technol.*, 2015, **223**, p 225–231. <https://doi.org/10.1016/j.jmatprotec.2015.04.006>
40. L. Han, M. Thornton, and M. Shergold, A Comparison of the Mechanical Behaviour of Self-Piercing Riveted and Resistance Spot Welded Aluminium Sheets for the Automotive Industry, *Mater. Des.*, 2010, **31**(3), p 1457–1467. <https://doi.org/10.1016/j.matdes.2009.08.031>
41. L. Han, A. Chrysanthou, and K. Young, Mechanical Behaviour of Self-Piercing Riveted Multi-Layer Joints Under Different Specimen Configurations, *Mater. Des.*, 2007, **28**(7), p 2024–2033. <https://doi.org/10.1016/j.matdes.2006.06.015>

Publisher's Note Springer Nature remains neutral with regard to jurisdictional claims in published maps and institutional affiliations.

Springer Nature or its licensor (e.g. a society or other partner) holds exclusive rights to this article under a publishing agreement with the author(s) or other rightsholder(s); author self-archiving of the accepted manuscript version of this article is solely governed by the terms of such publishing agreement and applicable law.